Group 4 Transition Metal−Benzene Adducts: Carbon Ring Deformation upon Complexation

Jonathan T. Lyon and Lester Andrews*

Chemistry Department, University of Virginia, P. O. Box 400319, Charlottesville, Virginia 22904-4319

Received: February 27, 2006; In Final Form: April 25, 2006

Benzene is reacted with titanium, zirconium, and hafnium metal atoms, which are produced by laser-ablation. The $M(C_6H_6)$, $M(C_6H_6)_2$, and $M_2(C_6H_6)_3$ complexes are formed, isolated in solid argon, and identified by infrared spectroscopy using isotopic substitution of the benzene precursor. Density functional theory (DFT) calculations are used to confirm molecular assignments. Based on computed energies and the observed vibrational spectra and isotopic shifts, electronic ground states and geometries are predicted. Observed splitting of formerly degenerate modes provides the first experimental evidence for deformation of the planar carbon skeleton of benzene upon complexation with early transition metal atoms.

Introduction

Interactions between transition metals and benzene are one of the fundamental building blocks of organometallic chemistry. The study of transition metal−benzene complexes also provides a basic understanding of similar interactions involved in surface science and catalysis, as well as bonding between transition metals and larger carbon molecules such as fullerenes.[1] Despite the wealth of knowledge concerning bisbenzene metal molecules, relatively little is known about reactive monobenzene $M(C_6H_6)$ complexes. Matrix isolation has proven to be a suitable way to form and isolate these metal−benzene complexes so that chemical properties can be investigated by such means as electron paramagnetic resonance (EPR),[2−5] electronic absorption,[2,6] Raman,[7] and infrared spectroscopies.[2,8−18] Early transition metal monobenzene $M(C_6H_6)$ complexes have previously been assumed to have C_{6v} symmetry. Only recently have theoretical calculations predicted that the planar carbon skeleton in these complexes might deform in select electronic states,[18,19] and even the ground states of several $M(C_6H_6)$ complexes have been predicted to have a symmetry lower than C_{6v}.[20] However, this has yet to be observed experimentally for a neutral early transition metal complex.

Bisbenzene $M(C_6H_6)_2$ compounds involving titanium, zirconium, and hafnium metal atoms have all been previously studied theoretically.[21−31] $Ti(C_6H_6)_2$ has been synthesized numerous times, and the properties have been studied by many methods including mass,[1,16,29,32,33] electron spin resonance (ESR),[34] NMR,[16,35] infrared,[14−16,35] X-ray diffraction,[36,37] photoionization, and photoelectron spectroscopies.[1,16,29,32−34] In addition, the electric dipole moments of $Ti(C_6H_6)_2$ and $Zr(C_6H_6)_2$ have been measured[24] indicating that these molecules have symmetric structures. Numerous theoretical studies have also been performed on the Group 4 monobenzene $M(C_6H_6)$ complexes.[25,27,29,38−41] However, there is disagreement regarding the properties of these complexes. For example, the ground electronic state of $Ti(C_6H_6)$ has been reported as having spin multiplicities of 3[25,38,40] and 5.[27,29,39,41] Few experimental studies have observed the $Ti(C_6H_6)$ complex,[28,40,42] and it is believed that this molecule has near C_{6v} symmetry.[40,42] Recently elegant vibrational spectroscopic studies have been performed on transition metal ion−benzene and dibenzene complexes in the gas phase.[43]

We report infrared spectra and density functional theoretical results on the reaction products of laser-ablated Ti, Zr, and Hf metal atoms and benzene in solid argon. We find that the $M(C_6H_6)$ and $M(C_6H_6)_2$ compounds are the major reaction products and report the first experimental evidence for the $Zr(C_6H_6)$ and $Hf(C_6H_6)$ complexes. Using our calculated energies and comparing the observed vibrational absorptions and isotopic shifts, particularly values for $^{13}C_6H_6$, to those computed, we comment on possible ground electronic states. The observed splitting of degenerate vibrational modes of the C_6H_6 precursor provides the first experimental evidence for deformation of the planar carbon skeleton of benzene upon early transition metal complexation.

Experimental and Theoretical Procedure

Our experimental setup has been described in detail elsewhere.[18,44] In brief, titanium (Goodfellow Metals), zirconium (Johnson-Matthey), and hafnium (Johnson-Matthey) metal atoms, produced by laser-ablation of a rotating target using a Nd:YAG laser (1064 nm, 10 Hz repetition, 10 ns pulse width), were co-deposited with benzene diluted in argon onto a CsI window cooled to approximately 7 K. Matrix samples were annealed to various temperatures (20−40 K) and subjected to broadband photolysis from a medium-pressure mercury arc lamp (Philips, 175 W) with the globe removed ($\lambda > 220$ nm). Benzene, isotopic samples [C_6D_6 (Cambridge Isotopic Laboratories; 99.6%) and $^{13}C_6H_6$ (Cambridge Isotopic Laboratories; 99%)], and select mixtures were purified through several freeze−pump−thaw cycles with liquid nitrogen prior to use in experiments. Fourier transform infrared spectra were collected at 0.5 cm^{-1} resolution on a Nicolet Magna 550 spectrometer with a Mercury Cadmium Telluride (MCT) type B detector cooled to 77 K.

Density functional theory (DFT) calculations were performed using the Gaussian 98 program to support molecular identifications.[45] The BPW91 and B3LYP functionals were used for all

* To whom correspondence should be addressed. E-mail: lsa@virginia.edu.

10.1021/jp061242+ CCC: $33.50
Published on Web 06/06/2006

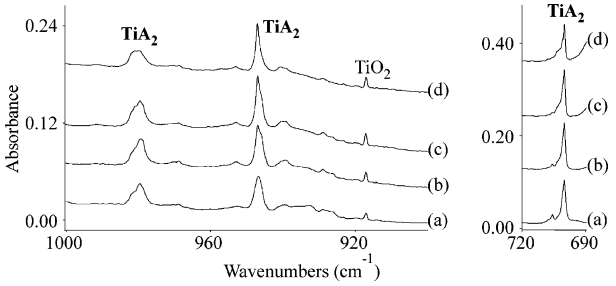

Figure 1. IR spectra in the 1000−900 and 720−690 cm^{-1} regions for (a) laser-ablated titanium co-deposited with benzene for 1 h and after annealing to (b) 30 K, (c) 35 K, and (d) 40 K. Absorptions labeled TiA_2 refer to the $Ti(C_6H_6)_2$ species.

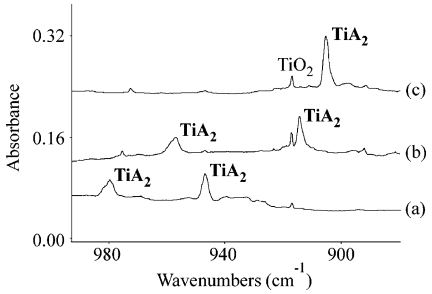

Figure 2. IR spectra in the 990−880 cm^{-1} region from co-depositing laser-ablated titanium with (a) C_6H_6, (b) $^{13}C_6H_6$, and (c) C_6D_6 for 1 h. Spectra were recorded after annealing to 40 K. Absorptions labeled TiA_2 correspond to the $Ti(C_6H_6)_2$ product.

calculations.[46,47] Unless otherwise noted, carbon and hydrogen atoms were represented by a 6-311++G(d,p) basis set,[48] whereas the SDD pseudopotential was used to represent the electronic density of the transition metal atoms.[49] Most calculations on the Group 4 $M(C_6H_6)$ complexes were confined to either C_{6v} or C_{2v} symmetries, whereas computations performed on $M(C_6H_6)_2$ compounds were constrained to D_{6h} or D_{6d} symmetries. In select instances the confined symmetries were reduced further. All energy values reported include zero-point vibrational corrections. The ΔE_{rxn} values were computed as the sum of the ground-state energies of the reactants (benzene molecules and transition metal atoms) minus the ground-state energy of the products.

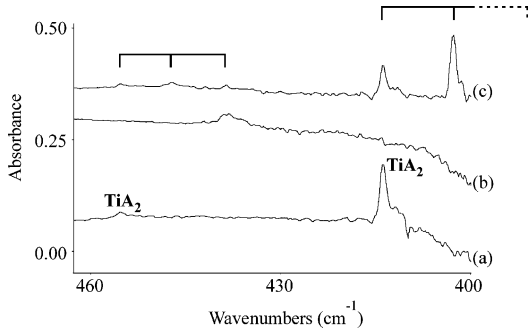

Figure 3. IR spectra in the 460−400 cm^{-1} region of the $Ti(C_6H_6)_2$ product (absorptions labeled TiA_2) formed when laser-ablated titanium reacted with (a) 0.5% C_6H_6, (b) 0.5% C_6D_6, and (c) a mixture of 0.2% C_6H_6 and 0.2% C_6D_6 in argon. Spectra were recorded after annealing to 40 K.

Results

Reactions of Group 4 transition metals with benzene in excess argon will be reported in turn.

Ti + C_6H_6. Dilute concentrations of benzene in Ar (0.1−0.5%) were co-deposited with Ti atoms. Product absorptions are shown in Figures 1−3 and compared with theoretically predicted vibrational results in Table 1. New absorptions corresponding to a reaction product observed at 413.7, 452.9, 700.0, 947.0, and 979.8 cm^{-1} increased in intensity on annealings up to 35 K, showed no change on photolysis, and decreased in intensity on annealing to 40 K. These absorptions are labeled TiA_2 in the figures. Weak impurity absorptions observed in our spectra at 766.2 (TiN_2), 917.1 and 946.9 (TiO_2), and 987.8 (TiO) have been previously reported.[50−52]

Zr + C_6H_6. Benzene in argon at different concentrations (0.02−1.5%) was reacted with zirconium atoms. Representative spectra are shown in Figures 4−7 and product absorptions are listed in Table 2. New absorptions corresponding to reaction products were separated into three groups based on behavior. Group A absorptions at 918.3, 940.9, 1368.7, and 1406.1 cm^{-1} increased in intensity slightly on annealings up to 35 K, decreased on photolysis, and decreased on further annealings. They are labeled ZrA in the figures. Group B absorptions at 682.4, 933.7, and 975.1 cm^{-1} increased in intensity on annealing

TABLE 1: Observed and Calculated Isotopic Frequencies (cm^{-1}) and Intensities (km/mol) at Different Levels for the $Ti(C_6H_6)_2$ Complex

BPW91/6-311++G(d,p)/SDD

symmetry/wilson number[53]	species	mode[a]	C_6H_6 obsd	C_6H_6 calcd	C_6H_6 intens	C_6D_6 obsd	C_6D_6 calcd	C_6D_6 intens	$^{13}C_6H_6$ obsd	$^{13}C_6H_6$ calcd	$^{13}C_6H_6$ intens
A_{2u}	$Ti(C_6H_6)_2$[b]	ν_a(MC)	413.7	399.9	(113)		378.1	(130)	410.7	396.8	(111)
E_{1u}		ν_t(MC)	452.9	441.1	(12)	437.0	426.0	(13)	447.9	434.1	(12)
A_{2u}/11		ν_{o-p}(CH)	700.0	692.0	(125)	540.5	532.0	(20)	696.8	688.8	(128)
A_{2u}/1		ν_s(CC)	947.0	938.4	(60)	905.4	897.1	(53)	914.3	905.2	(54)
E_{1u}/18		ν_{i-p}(CH)	979.8	974.1	(34)	786.6	775.9	(17)	957.2	953.2	(32)
E_{1u}/19		ν(CC)		1397.1	(0)	1250.9	1237.4	(6)		1371.9	(1)

B3LYP/6-311++G(d,p)/SDD

symmetry/wilson number[53]	species	mode[a]	C_6H_6 obsd	C_6H_6 calcd	C_6H_6 intens	C_6D_6 obsd	C_6D_6 calcd	C_6D_6 intens	$^{13}C_6H_6$ obsd	$^{13}C_6H_6$ calcd	$^{13}C_6H_6$ intens
A_{2u}	$Ti(C_6H_6)_2$[b]	ν_a(MC)	413.7	393.0	(149)		375.6	(160)	410.7	389.9	(147)
E_{1u}		ν_t(MC)	452.9	443.1	(14)	437.0	428.9	(15)	447.9	436.1	(14)
A_{2u}/11		ν_{o-p}(CH)	700.0	721.8	(110)	540.5	549.0	(16)	696.8	718.6	(113)
A_{2u}/1		ν_s(CC)	947.0	960.3	(64)	905.4	917.8	(57)	914.3	926.3	(58)
E_{1u}/18		ν_{i-p}(CH)	979.8	998.3	(33)	786.6	797.2	(17)	957.2	976.7	(32)
E_{1u}/19		ν(CC)		1443.7	(0)	1250.9	1275.1	(6)		1417.9	(1)

[a] Vibrational modes: ν_a(MC) = antisymmetric metal−carbon mode; ν_t(MC) = antisymmetric tilting; ν_{o-p}(CH) = C−H out-of-plane bending; ν_s(CC) = symmetric C−C stretching; ν_{i-p}(CH) = C−H in-plane rocking; ν(CC) = antisymmetric C−C stretching. [b] Theoretical results: $^1A_{1g}$ ground electronic state (D_{6h} symmetry).

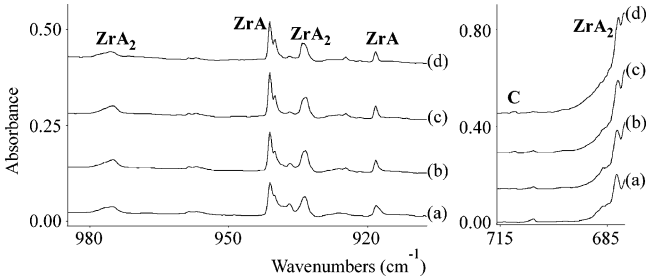

Figure 4. IR spectra in the 980−900 and 715−680 cm^{-1} regions for (a) co-depositing laser-ablated zirconium with C_6H_6 for 1 h and after annealing to (b) 30 K, (c) 35 K, and (d) 40 K. Absorptions labeled ZrA refer to the $Zr(C_6H_6)$ product, ZrA_2 corresponds to the $Zr(C_6H_6)_2$ product, and C are for the $Zr_2(C_6H_6)_3$ product.

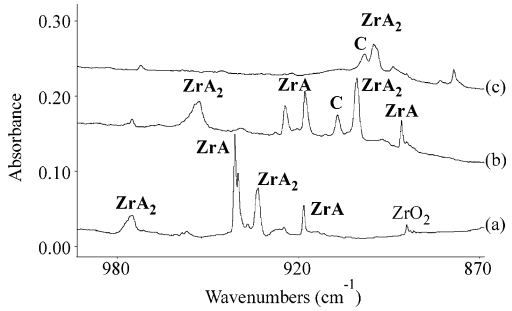

Figure 5. IR spectra in the 990−870 cm^{-1} region from co-depositing laser-ablated zirconium with (a) C_6H_6, (b) $^{13}C_6H_6$, and (C) C_6D_6 for 1 h. Spectra were recorded after annealing to 35 K. Absorptions labeled ZrA refer to the $Zr(C_6H_6)$ product, ZrA_2 corresponds to the $Zr(C_6H_6)_2$ product, and C are for the $Zr_2(C_6H_6)_3$ product.

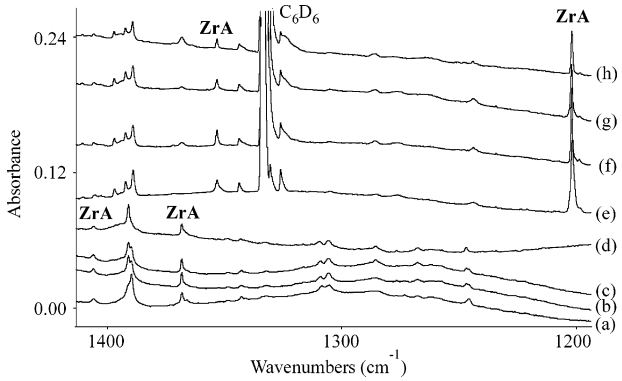

Figure 6. IR spectra in the 1410−1200 cm^{-1} region from (a) co-depositing laser-ablated zirconium with C_6H_6 for 1 h and after the resulting matrix was subjected to (b) annealing to 35 K, (c) full arc photolysis, and (d) annealing to 40 K. IR spectra after (e) zirconium was reacted with C_6D_6 for 1 h and the resulting matrix was subjected to (f) annealing to 35 K, (g) full arc photolysis, and (h) annealing to 40 K. Absorptions labeled ZrA refer to the $Zr(C_6H_6)$ product.

to 20 K, decreased on further annealings, and increased during photolysis. Group B absorptions are labeled ZrA_2 in the figures. Group C absorptions at 711.1 and 939.8 cm^{-1} increased on all annealings, decreased slightly on photolysis, and are labeled C in the figures. Trace impurity absorptions observed at 706.3 (NZrN), 818.0 and 884.3 (ZrO_2), 958.6 (ZrO), and 1022.8 cm^{-1} ($Zr(N_2)$) have been previously reported.[50,52]

Hf + C_6H_6. Ranges of benzene concentrations (0.1−0.5%) in argon were employed with laser-ablated hafnium atoms. New product absorptions were separated into two groups based on behavior. They are shown in Figures 8−10 and the frequencies are listed in Table 3. Group A absorptions observed at 910.2 and 930.2 cm^{-1} increased in intensity on all annealings up to 35 K, decreased on photolysis, and increased on further

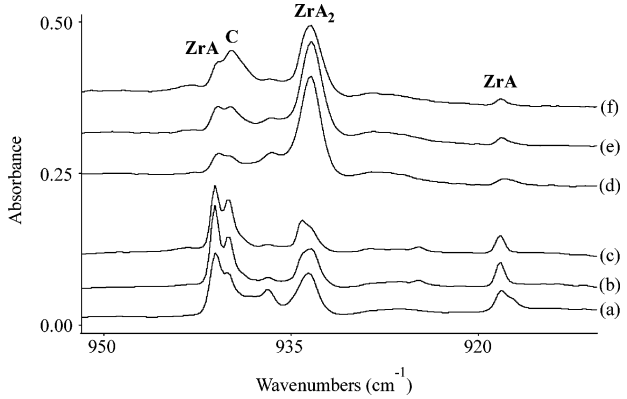

Figure 7. IR spectra in the 950−910 cm^{-1} region for (a) co-depositing laser-ablated zirconium with 0.5% C_6H_6 and after annealing to (b) 35 K and (c) 40 K, compared to spectra recorded after (d) co-depositing laser-ablated zircoinium with 1.5% C_6H_6 and annealing to (e) 35 K and (f) 40 K. Absorptions labeled ZrA refer to the $Zr(C_6H_6)$ product, ZrA_2 corresponds to the $Zr(C_6H_6)_2$ product, and C are for the $Zr_2(C_6H_6)_3$ product.

annealing. These absorptions are labeled HfA in the figures. Group B absorptions at 688.2, 928.8, and 969.9 cm^{-1} increased on all annealings and showed little or no effect from photolysis. These absorptions are labeled HfA_2 in the figures. Previously identified impurity absorption peaks at 708.1 (NHfN), 805.3, 807.6, 814.0, and 816.0 (HfO_2: ν_3), 883.4 (HfO_2: ν_1), and 958.3 cm^{-1} (HfO) were also observed in our spectra.[50,52]

Discussion

$Ti(C_6H_6)_2$. Since titanium vapor has been reacted with benzene in solid argon previously,[14−16] we now only describe differences between our results and those previously reported, and discuss new assignments based on isotopic substitution. Four of the five observed absorptions at 413.7, 452.9, 700.0, 947.0, and 979.8 cm^{-1} are in good agreement with previous experimental peaks at 411, 452, 946, and 979 cm^{-1} corresponding to the $Ti(C_6H_6)_2$ molecule in solid argon.[15,16] As no definitive vibrational assignments were made in these previous studies, we use our observed isotopic shifts to comment on the nature of these modes.

The absorption at 452.9 cm^{-1} shows a larger carbon-13 shift and is a higher frequency than the absorption at 413.7 cm^{-1}. This is similar to the absorptions observed in this region for the $V(C_6H_6)_2$ compound,[18] and the trend is supported by our theoretical predictions (Table 1). In addition, when a mixture of benzene and deuterated benzene was reacted with Ti atoms, two new absorptions appeared at 402.6 and 447.1 cm^{-1} between the $Ti(C_6H_6)_2$ and $Ti(C_6D_6)_2$ absorptions in a 1:2:1 relative intensity pattern (the lower $Ti(C_6D_6)$ band expected near 392 cm^{-1} is below our instrumental limits, Figure 3), confirming that these absorptions correspond to vibrational modes of a bisbenzene product. Hence, the absorptions at 413.7 and 452.9 cm^{-1} are assigned to the antisymmetric metal−carbon vibrational mode (abbreviated ν_a(MC)) and antisymmetric tilting mode (abbreviated ν_t(MC)) of the $Ti(C_6H_6)_2$ compound, respectively.

The two absorptions at 947.0 and 979.8 cm^{-1} show drastically different isotopic shifts (Table 1). Vibrational modes that are expected to be observed in this area include the symmetric carbon−carbon stretching mode (abbreviated ν_s(CC)) and the carbon−hydrogen in-plane rocking mode (abbreviated ν_{i-p}(CH)). As the absorption at 947.0 cm^{-1} shows a large carbon-13 shift and a relatively small deuterium shift (Figure 2), we assign this

TABLE 2: Observed and Calculated Isotopic Frequencies (cm^{-1}) and Intensities (km/mol) at Different Levels of Theory for the $Zr(C_6H_6)$, $Zr(C_6H_6)_2$, and $Zr_2(C_6H_6)_3$ Complexes

BPW91/6-311++G(d,p)/SDD

symmetry/wilson number[53]	species	mode[a]	C_6H_6 obsd	C_6H_6 calcd	C_6H_6 intens	C_6D_6 obsd	C_6D_6 calcd	C_6D_6 intens	$^{13}C_6H_6$ obsd	$^{13}C_6H_6$ calcd	$^{13}C_6H_6$ intens
$A_1/11$	$Zr(C_6H_6)$[b]	ν_{o-p}(CH)		712.3	(0)	533.7	555.1	(14)		708.9	(0)
$A_1/1$		ν_s(CC)	918.3	909.7	(5)		874.0	(4)	885.8	877.4	(4)
$B_2/18$		ν_{i-p}(CH)	940.9	916.0	(25)	763.8	745.1	(15)	917.9	894.3	(23)
$B_1/18$		ν_{i-p}(CH)		953.9	(7)		758.0	(4)	924.4	932.7	(7)
$B_2/19$		ν(CC)	1368.7	1364.7	(0)	1201.9	1182.4	(8)		1343.3	(0)
$B_1/19$		ν(CC)	1406.1	1407.9	(14)	1353.6	1362.4	(32)	1365.6	1370.6	(8)
$A_{2u}/11$	$Zr(C_6H_6)_2$[c]	ν_{o-p}(CH)	682.4	675.5	(114)		506.0	(35)		672.8	(117)
$A_{2u}/1$		ν_s(CC)	933.7	927.5	(86)	894.6	886.0	(79)	900.9	894.3	(79)
$E_{1u}/18$		ν_{i-p}(CH)	975.1	962.6	(38)	780.5	768.2	(21)	953.2	941.6	(37)
$A_{2u}/11$	$Zr_2(C_6H_6)_3$[c]	ν_{o-p}(CH)	711.1	678.1[d]	(124)[d]	527.4	508.9[d]	(19)[d]	709.1	675.3[d]	(128)[d]
$A_{2u}/1$		ν_s(CC)	939.8	925.3[d]	(161)[d]	898.2	883.8[d]	(152)[d]	907.2	892.2[d]	(146)[d]

B3LYP/6-311++G(d,p)/SDD

symmetry/wilson number[53]	species	mode[a]	C_6H_6 obsd	C_6H_6 calcd	C_6H_6 intens	C_6D_6 obsd	C_6D_6 calcd	C_6D_6 intens	$^{13}C_6H_6$ obsd	$^{13}C_6H_6$ calcd	$^{13}C_6H_6$ intens
$A_1/11$	$Zr(C_6H_6)$[b]	ν_{o-p}(CH)		728.9	(30)	533.7	529.7	(39)		725.5	(31)
$A_1/1$		ν_s(CC)	918.3	928.0	(21)		893.2	(16)	885.8	895.1	(18)
$B_2/18$		ν_{i-p}(CH)	940.9	937.5	(28)	763.8	763.8	(16)	917.9	915.6	(26)
$B_1/18$		ν_{i-p}(CH)		979.6	(7)		781.3	(4)	924.4	957.5	(6)
$B_2/19$		ν(CC)	1368.7	1412.6	(0)	1201.9	1220.1	(10)		1390.7	(0)
$B_1/19$		ν(CC)	1406.1	1450.1	(12)	1353.6	1389.3	(35)	1365.6	1414.8	(7)
$A_{2u}/11$	$Zr(C_6H_6)_2$[c]	ν_{o-p}(CH)	682.4	704.6	(99)		526.1	(27)		701.9	(102)
$A_{2u}/1$		ν_s(CC)	933.7	946.0	(101)	894.6	903.7	(92)	900.9	912.2	(93)
$E_{1u}/18$		ν_{i-p}(CH)	975.1	985.0	(44)	780.5	789.1	(23)	953.2	963.1	(42)
$A_{2u}/11$	$Zr_2(C_6H_6)_3$[c]	ν_{o-p}(CH)	711.1	711.1[d]	(75)[d]	527.4	566.6[d]	(47)[e]	709.1	708.3[d]	(81)[d]
$A_{2u}/1$		ν_s(CC)	939.8	945.6[d]	(183)[d]	898.2	903.2[d]	(173)[e]	907.2	911.8[d]	(166)[d]

[a] Vibrational Modes: ν_{o-p}(CH) = C−H out-of-plane bending; ν_s(CC) = symmetric C−C stretching; ν_{i-p}(CH) = C−H in-plane rocking; ν(CC) = antisymmetric C−C stretching. [b] Theoretical results: $^3A_2$ ground electronic state (C_{2v} symmetry). [c] Theoretical results: $^1A_{1g}$ ground electronic state (D_{6h} symmetry). [d] 6-31G(d)/SDD basis sets were used to calculate these frequencies and intensities.

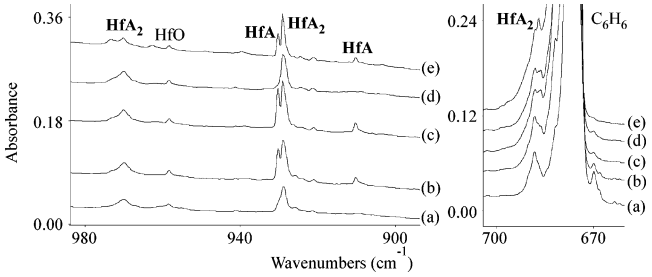

Figure 8. IR spectra in the 980−900 and 700−660 cm^{-1} regions for (a) co-depositing laser-ablated hafnium with C_6H_6 for 1 h and after (b) annealing to 30 K (c) and 35 K, (d) full-arc photolysis for 15 min, and (e) annealing to 40 K. Absorptions labeled HfA refer to the $Hf(C_6H_6)$ product, and HfA_2 corresponds to the $Hf(C_6H_6)_2$ product.

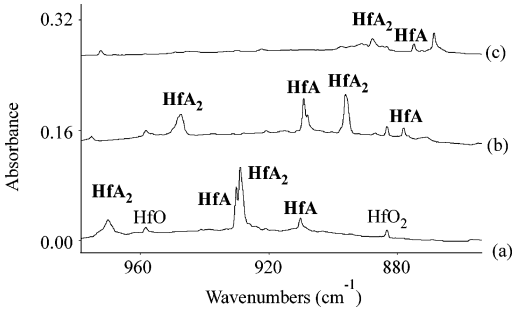

Figure 9. IR spectra in the 970−860 cm^{-1} region from co-depositing laser-ablated hafnium with (a) C_6H_6, (b) $^{13}C_6H_6$, and (C) C_6D_6 for 1 h. Spectra were recorded after annealing to 35 K. Absorptions labeled HfA refer to the $Hf(C_6H_6)$ product, and HfA_2 corresponds to the $Hf(C_6H_6)_2$ product.

frequency to the ν_s(CC) mode. Note that this value of 947.0 cm^{-1} is between the values of 946 and 949 cm^{-1} reported previously in argon matrix experiments,[14−16] above the value of 943 cm^{-1} reported in a KBr pellet,[35] and in agreement with the recent 946 cm^{-1} measurement for $Ti(C_6H_6)_2^+$ in the gas phase.[43] The infrared absorption at 979.8 cm^{-1}, which shows a larger H/D ratio (1.246), is assigned to the ν_{i-p}(CH) mode of the $Ti(C_6H_6)_2$ molecule. This mode is slightly lower than the 992 cm^{-1} assignment for the Ti^+−dibenzene complex.[43]

The carbon−hydrogen out-of-plane bending vibration (abbreviated ν_{o-p}(CH)) was not detected in previous argon matrix work.[15,16] We observe an absorption at 700.0 cm^{-1} that shows the same product behavior as the other observed modes of the $Ti(C_6H_6)_2$ molecule (Figure 1). This frequency is in good agreement with an absorption observed in a KBr pellet at 694 cm^{-1} corresponding to the $Ti(C_6H_6)_2$ molecule,[35] but substantially lower than the recent 739 cm^{-1} value for the gas-phase ion complex.[43] We expect the cation complex to be more strongly bound and to blue-shift the out-of-plane C−H benzene mode more than the neutral complex. The observed large deuterium shift and small carbon-13 shift indicate that this absorption corresponds to the ν_{o-p}(CH) bending mode of this $Ti(C_6H_6)_2$ compound.

Although no other vibrational modes of the $Ti(C_6H_6)_2$ compound were observed, we did observe an absorption in experiments performed with deuterated benzene at 1250.9 cm^{-1} showing similar behavior. This absorption is in the region where we expect the deuterated antisymmetric carbon−carbon stretching mode (abbreviated ν(CC)) to be observed. As our calcula-

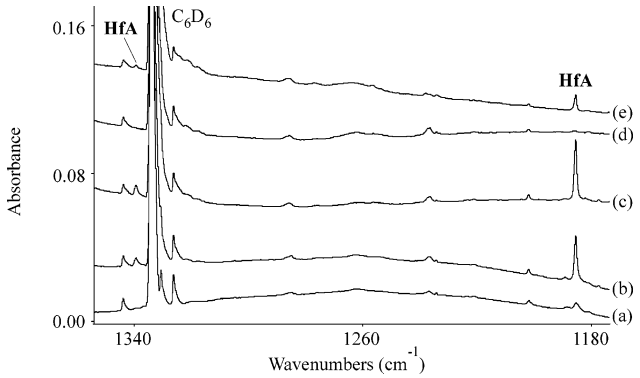

Figure 10. IR spectra in the 1350−1170 cm^{-1} region from (a) co-depositing laser-ablated hafnium with C_6D_6 for 1 h and after (b) annealing to 30 K (c) and 35 K, (d) full-arc photolysis for 15 min, and (e) annealing to 40 K. Absorptions labeled HfA refer to the $Hf(C_6H_6)$ product.

tions predicted this vibrational mode to be the most infrared active for the $Ti(C_6D_6)_2$ isotopomer, this assignment is appropriate.

$Zr_n(C_6H_6)_x$ ($n = 1$, $x = 1, 2$; $n = 2$, $x = 3$). When zirconium was reacted with dilute benzene in argon, four absorptions were observed between 900 and 1000 cm^{-1} at 918.3, 933.7, 940.9, and 975.1 cm^{-1} showing either group A or B behavior (Figure 4). Isotopic counterparts of these absorptions indicate that they correspond to two sets of ν_s(CC) and ν_{i-p}(CH) vibrational modes (Figure 5). The group B absorptions at 933.7 and 975.1 cm^{-1} are at a higher frequency than the two group A absorptions. In addition, the group A ν_s(CC) vibration at 918.3 cm^{-1} shows a larger isotopic carbon-13 shift than the group B vibration at 933.7 cm^{-1}, and the group B ν_{i-p}(CH) rocking vibration at 975.1 cm^{-1} exhibits a larger deuterium shift than the group A absorption at 940.9 cm^{-1} (Table 2). These trends are consistent with those previously observed with Group 5 metal−benzene complexes[18] and correspond to assigning the group A absorptions to the $Zr(C_6H_6)$ complex and group B absorptions to $Zr(C_6H_6)_2$. Although we do not observe the deuterium counterpart of the ν_s(CC) mode of the $Zr(C_6H_6)$ complex, it should appear in the spectrum near the ZrO_2 impurity absorption at 884.3 cm^{-1} and is probably hidden by this peak. The carbon-13 isotopic counterpart of the absorption at 940.9 cm^{-1} is split into two peaks observed at 917.9 and 924.4 cm^{-1}. We believe the most likely explanation for this observed splitting is that the ν_{i-p}(CH) vibrational mode has lost the double degeneracy (complex symmetry reduction beyond C_{3v}) and that each of the resulting new vibrational splittings shows a unique carbon-13 shift. Each splitting has different IR intensities and the infrared intensity of each splitting should be affected differently with carbon-13 substitution. Both mode splittings are mixed, and we feel that symmetry reduction out of C_{6v} is the most likely explanation of the splitting observed for this ν_{i-p}(CH) mode of the $Zr(C_6H_6)$ complex.

An absorption at 682.4 cm^{-1} showed group B behavior. Although no isotopic counterparts were observed for this vibration, it is only slightly blue-shifted from the ν_{o-p}(CH) bending vibration of the benzene precursor at 674.6 cm^{-1}. The deuterium and carbon-13 counterparts of this mode were predicted to overlap with the observed isotopic benzene precursor absorptions and aggregate bands. Both of our theoretical methods predicted this ν_{o-p}(CH) bending vibration of the $Zr(C_6H_6)_2$ complex to red-shift from the same vibrational mode of the $Ti(C_6H_6)_2$ molecule. This absorption at 682.4 cm^{-1} is red-shifted by 17.6 cm^{-1} from the ν_{o-p}(CH) mode of the $Ti(C_6H_6)_2$ compound, in good agreement with these theoretical predictions. Hence, we assign this vibration to the ν_{o-p}(CH) mode of the $Zr(C_6H_6)_2$ molecule.

Although the ν_{o-p}(CH) mode of the $Zr(C_6H_6)$ complex was not found in our spectra, we have observed the deuterated counterpart at 533.7 cm^{-1}, which shows group A behavior. For

TABLE 3: Observed and Calculated Isotopic Frequencies (cm^{-1}) and Intensities (km/mol) at Different Levels of Theory for the $Hf(C_6H_6)$ and $Hf(C_6H_6)_2$ Complexes

BPW91/6-311++G(d,p)/SDD

symmetry/wilson number[53]	species	mode[a]	C_6H_6			C_6D_6			$^{13}C_6H_6$		
			obsd	calcd	intens	obsd	calcd	intens	obsd	calcd	intens
A_1/11	$Hf(C_6H_6)$[b]	ν_{o-p}(CH)		718.6	(151)	530.5	550.3	(89)		715.5	(52)
A_1/1		ν_s(CC)	910.2	918.2	(3)	874.9	883.1	(3)	878.1	885.6	(2)
B_2/18		ν_{i-p}(CH)	930.2	924.7	(25)	755.4	750.3	(15)	909.0	902.6	(23)
B_1/18		ν_{i-p}(CH)		973.2	(7)		766.5	(4)		952.5	(7)
B_2/19		ν(CC)		1374.4	(0)	1185.3	1194.8	(4)		1352.3	(0)
B_1/19		ν(CC)		1431.9	(6)	1339.7	1390.5	(17)		1391.3	(3)
A_{2u}/11	$Hf(C_6H_6)_2$[c]	ν_{o-p}(CH)	688.2	674.4	(130)		504.3	(30)	684.8	671.7	(132)
A_{2u}/1		ν_s(CC)	928.8	921.8	(90)	888.1	880.6	(82)	895.9	888.7	(83)
E_{1u}/18		ν_{i-p}(CH)	969.9	960.8	(44)	776.8	767.5	(23)	947.5	939.7	(41)

B3LYP/6-311++G(d,p)/SDD

symmetry/wilson number[53]	species	mode[a]	C_6H_6			C_6D_6			$^{13}C_6H_6$		
			obsd	calcd	intens	obsd	calcd	intens	obsd	calcd	intens
A_1/11	$Hf(C_6H_6)$[b]	ν_{o-p}(CH)		742.0	(124)	530.5	568.9	(80)		738.5	(120)
A_1/1		ν_s(CC)	910.2	933.9	(5)	874.9	900.2	(4)	878.1	900.9	(4)
B_2/18		ν_{i-p}(CH)	930.2	943.6	(27)	755.4	767.7	(16)	909.0	921.1	(25)
B_1/18		ν_{i-p}(CH)		996.8	(7)		789.3	(4)		975.0	(6)
B_2/19		ν(CC)		1419.9	(0)	1185.3	1229.4	(4)		1397.6	(0)
B_1/19		ν(CC)		1470.7	(8)	1339.7	1414.7	(17)		1432.4	(2)
A_{2u}/11	$Hf(C_6H_6)_2$[c]	ν_{o-p}(CH)	688.2	708.1	(109)		527.1	(36)	684.8	705.4	(111)
A_{2u}/1		ν_s(CC)	928.8	941.6	(107)	888.1	899.5	(98)	895.9	907.8	(99)
E_{1u}/18		ν_{i-p}(CH)	969.9	984.8	(41)	776.8	788.9	(23)	947.5	962.9	(39)

[a] Vibrational Modes: ν_{o-p}(CH) = C−H out-of-plane bending; ν_s(CC) = symmetric C−C stretching; ν_{i-p}(CH) = C−H in-plane rocking; ν(CC) = antisymmetric C−C stretching. [b] Theoretical results: $^3A_2$ ground electronic state (C_{2v} symmetry). [c] Theoretical results: $^1A_{1g}$ ground electronic state (D_{6h} symmetry).

Group 5 M(C_6H_6) complexes (which have C_{6v} symmetry) the ν_{o-p}(CH) mode of the deuterated complex was the weakest infrared absorber compared to other isotopomers.[18] However, for the Zr(C_6H_6) complex the ν_{o-p}(CH) mode of the deuterated complex is computed to be considerably more infrared active compared to the other two isotopomers when the symmetry is reduced to C_{2v} (Table 2). Hence, the observation of this vibrational mode in only experiments performed with deuterated benzene is possible further evidence for reduction of complex symmetry below C_{3v}.

Two absorptions were observed at 1368.7 and 1406.1 cm^{-1} showing group A behavior. The deuterated analogs of these modes were stronger infrared absorbers at 1201.9 and 1353.6 cm^{-1} (Figure 6). Only one carbon-13 splitting was observed at 1365.6 cm^{-1}. The ν(CC) mode was always observed to be the most infrared active for the deuterated counterparts of Group 5 M(C_6H_6) complexes.[18] As the ν(CC) mode is doubly degenerate for the benzene precursor, this mode should be split only if the carbon skeleton of benzene is deformed during complexation with zirconium atoms. Given the correlation between these observed absorptions, their isotopic counterparts, and those predicted for the Zr(C_6H_6) complex (Table 2), we assign these two frequencies to different splittings of the ν(CC) mode of this zirconium−benzene complex and propose this observed splitting as convincing evidence for carbon ring deformation during zirconium complexation.

The absorption at 711.1 cm^{-1} showed group C behavior, and its isotopic shifts are consistent with a ν_{o-p}(CH) bending mode (Table 2). Also, the isotopic counterparts of another group C vibration are observed at 907.2 ($^{13}C_6H_6$) and 898.2 cm^{-1} (C_6D_6) as shown in Figure 5. This vibration was not seen in experiments with C_6H_6 until the benzene concentration was increased to 1.5%. In this experiment, an absorption grew in at 939.8 cm^{-1} on top of the ν_{i-p}(CH) rocking vibration of the Zr(C_6H_6) complex at 940.9 cm^{-1} (Figure 7) showing group C behavior. These isotopic shifts are consistent with a ν_s(CC) ring stretching vibration. Also notice in Figure 7 that while the Zr(C_6H_6)$_2$ molecule is created in larger abundance in the higher benzene concentration experiment, the population of the monobenzene Zr(C_6H_6) complex decreases.

Since the group C peaks grow on annealings and decrease on photolysis, these absorptions probably correspond to higher aggregate species. A number of other possibilites can be ruled out. No absorptions were observed that could correspond to a Zr−H stretching mode, which would be intense if a C−H insertion product were formed. The observation that group C absorptions grew substantially when the benzene concentration was increased to 1.5% indicates that the molecule is not Zr_2(C_6H_6). We also considered a hydrogen elimination product, namely an η^1-Zr(C_6H_5) compound with C_{2v} symmetry. However, calculations for this molecule also failed to predict an accurate representation of the observed spectrum. The presence of ν_{o-p}(CH) and ν_s(CC) modes indicate that the carbon skeleton of the benzene ring remains intact. We considered the secondary addition product $Zr_2(C_6H_6)_3$, since this complex has been formed with many first row transition metals in gas-phase experiments.[1,28,29,32,33,54−57] As only one ν_s(CC) mode was observed, we modeled this compound with D_{6h} symmetry to produce only one infrared active ν_s(CC) mode. Although only two absorptions were observed for this complex, good correlation with those predicted (Table 2) are in accord with this possible assignment. In particular, the observed absorptions are the same as the two modes predicted to be the most infrared active. The calculated frequencies of the $Zr_2(C_6H_6)_3$ molecule cannot be directly compared to those of the other complexes since they were computed with different basis functions. A simple optimization of the $Zr_2(C_6H_6)_3$ molecule using the same theoretical method used for all other complexes predicted a decrease in the C−C bond lengths. This would slightly increase the ν_s(CC) mode as found here.

Hf(C_6H_6)$_x$ (x = 1, 2). When hafnium is reacted with benzene a new product absorption is observed at 688.2 cm^{-1} showing group B behavior. Given the location of this absorption and the observed $^{12}C/^{13}C$ isotopic ratio, this absorption is assigned to the ν_{o-p}(CH) mode of the Hf(C_6H_6)$_2$ complex in good agreement with theoretical predictions (Table 3). Notice this vibrational mode is blue-shifted by only 6 cm^{-1} from the Zr(C_6H_6)$_2$ compound absorption, which was red-shifted from the Ti(C_6H_6)$_2$ absorption.

Two group A absorptions and two group B absorptions are observed in the 900−1000 cm^{-1} region (Figure 8). The observed isotopic shifts (Figure 9) are consistent with these four absorptions corresponding to two sets of ν_s(CC) and ν_{i-p}(CH) vibrational modes. The group A absorptions at 910.2 and 930.2 cm^{-1} are lower in frequency than the group B bands at 928.8 and 969.9 cm^{-1}. Also, the $^{12}C/^{13}C$ isotopic ratio of the ν_s(CC) stretching mode of the Hf(C_6H_6) complex is almost identical to that of the Hf(C_6H_6)$_2$ compound, and the deuterium shift in the ν_{i-p}(CH) mode of the bisbenzene molecule is slightly larger than that of the monobenzene complex (Table 3). These trends match what was observed in the experiments with zirconium. Hence, the group A absorptions are assigned to the Hf(C_6H_6) complex and the group B bands to Hf(C_6H_6)$_2$.

Although no other product absorptions were observed when experiments were performed with C_6H_6, other peaks were seen when deuterated benzene was used in the experiments. One group A absorption was observed at 530.5 cm^{-1}, and we assign this absorption to the ν_{o-p}(CH) mode of the Hf(C_6D_6) complex. This vibration is red-shifted from the Zr(C_6D_6) complex absorption by 3.2 cm^{-1}, giving good agreement with the BPW91 predicted 4.8 cm^{-1} shift. Interestingly, we observe this vibrational mode with C_6D_6 but not with C_6H_6. However, our calculations predicted the opposite order for the relative infrared intensity of these two isotopic compounds. Remember that this ν_{o-p}(CH) vibration of the Zr(C_6H_6) complex was only observed for the deuterated isotopomer and that the calculated infrared intensities supported that observation. This could indicate that the calculated infrared intensities of the ν_{o-p}(CH) mode of the Hf(C_6H_6) complex are in error. Another possibility is that the shift of this vibrational mode from that of the benzene precursor is overestimated by our calculations. Indeed the observed deuterium absorption is at a larger frequency than that predicted by both theoretical methods (Table 3). Hence, this mode of the Hf(C_6H_6) and Hf($^{13}C_6H_6$) isotopomers probably were not observed as they were covered by precursor absorptions.

The other two peaks observed in the deuterated spectra are at 1185.3 and 1339.7 cm^{-1} showing group A behavior (Figure 10). These absorptions are in the same region as the observed absorptions of the ν(CC) modes of the Zr(C_6D_6) complex at 1201.9 and 1353.6 cm^{-1}. Our computed frequencies and infrared intensities predict these vibrational modes to be quite intense in this region and support the assignment of these two absorptions at 1185.3 and 1339.7 cm^{-1} to the ν(CC) antisymmetric stretching mode of the Hf(C_6D_6) complex (Table 3). The observed splitting of this mode again confirms that the Hf(C_6H_6) complex has a symmetry lower than C_{3v}.

Ground Electronic States and Geometries. Bisbenzene transition metal sandwich compounds have been more widely

TABLE 4: A Comparison of Theoretically Predicted and Experimentally Determined Bond Lengths (Å) of the $Ti(C_6H_6)_2$ Molecule

method	Ti−C	Ti−Bz[a]	C−C	C−H	ref
HF	2.305		1.424	1.068	21
HF		1.764	1.415	1.072	28
MP2		1.694	1.40[b]	1.10[b]	25
MP2		1.721	1.443	1.089	28
CCSD(T)		1.728	1.451	1.10	22
DFT		1.742	1.430	1.09	23
DFT ZORA		1.751	1.429	1.09	22
DFT ZORA + ESA		1.753	1.432	1.09	22
LDA	2.212				26
PW91	2.256				26
B3LYP	2.29				24
B3LYP		1.741	1.430	1.084	28
BPW91	2.251	1.736	1.432	1.088	this work
B3LYP	2.259	1.753	1.425	1.081	this work
exptl	2.217−2.247				26,37

[a] Distance between the titanium atom and the center of the benzene ring. [b] Values held constant during optimization.

studied than the monobenzene $M(C_6H_6)$ complexes, and we discuss our results for these larger complexes first.

As evident in Table 4, the geometry of $Ti(C_6H_6)_2$ has been widely studied in the literature. Experimentally this molecule is known to have no permanent dipole and hence a symmetrical structure,[24] eliminating the possibility of ring bending. We performed calculations on the $Ti(C_6H_6)_2$ molecule in both D_{6h} and D_{6d} symmetries. Our BPW91 results predicted the D_{6h} symmetry to be lower in energy than the D_{6d} structure by less than 1 kcal/mol. B3LYP results predicted the D_{6d} structure to be slightly more than 2 kcal/mol lower in energy than the D_{6h} symmetry. Both isomers appear to have nearly identical energies, and accordingly different theoretical methods predict one or the other as the lowest energy structure. However, for the remainder of this discussion we assume a D_{6h} structure since it has been previously reported as the geometry[1,21−25,28,33] and it allows for comparison with Group 5 $M(C_6H_6)_2$ compounds.

In the case of the $V(C_6H_6)_2$ complex, we found that most theoretical methods overestimated the experimental V−C and V−Bz lengths, with the exception of a MP2 calculation which underestimated them.[18] In looking at Table 4, we see that all the methods with the exception of a LDA calculation predicted similar Ti−C distances (2.25−2.31 Å). All of these values are slightly larger than the experimental value (2.217−2.247 Å) determined by X-ray diffraction.[26,37] While DFT methods predicted Ti−Bz distances of 1.74−1.76 Å, HF calculations predicted longer distances (1.76−1.81 Å) and the MP2 and CCSD(T) methods predicted shorter Ti−Bz distances (1.69−1.73 Å). Accordingly, the C−C bond lengths vary slightly between methods. A comparison of our calculated vibrational frequencies and isotopic shifts to those observed for the $Ti(C_6H_6)_2$ compound is given in Table 1, showing good agreement between our theoretical and experimental results. The ΔE_{rxn} for the $Ti(C_6H_6)_2$ molecule was calculated as 109 and 72 kcal/mol using the BPW91 and B3LYP methods, respectively, indicating this product is energetically favorable to form. Although an all electron basis set on titanium might provide more accurate theoretical results, we employed the SDD pseudopotential to allow for comparison with the heavier Group 4 analogues and to include relativistic effects.

The $Zr(C_6H_6)_2$ complex has also been studied theoretically,[21−25] and experimental evidence indicates this molecule also has a symmetrical structure.[24] However, no theoretical studies that we are aware of have investigated a possible D_{6d} symmetry for this compound. Therefore, we performed calculations on this molecule imposing D_{6h} and D_{6d} symmetries. Our B3LYP calculations predicted the D_{6h} symmetry to have the lowest energy, with the D_{6d} symmetry lying slightly over 1 kcal/mol higher in energy, and our BPW91 computations predicted the D_{6h} symmetry to be less than 1 kcal/mol lower in energy than the D_{6d} structure. Hence, it seems likely that the $Zr(C_6H_6)_2$ compound has D_{6h} symmetry. We also investigated the possibility of D_{2d} symmetry, but these calculations converged to a D_{6d} structure. As the singlet state has been previously predicted as the ground electronic state of this molecule,[23−25] and as the singlet ground state is known experimentally for the $Ti(C_6H_6)_2$ compound,[34] we assumed this state for the $Zr(C_6H_6)_2$ molecule.

Our theoretical results predicted a ΔE_{rxn} of 129 and 96 kcal/mol using the BPW91 and B3LYP functionals for the $Zr(C_6H_6)_2$ compound, respectively. Both of these energies are larger than those predicted for the $Ti(C_6H_6)_2$ compound, showing that formation of the zirconium bisbenzene product is more energetically favorable than the titanium counterpart. Our computations predicted Zr−C bond distances of 2.431 and 2.439 Å, Zr−Bz distances of 1.964 and 1.978 Å, and C−C bond distances of 1.433 and 1.427 Å using the BPW91 and B3LYP methods, respectively. Although no structural information has been experimentally determined for the $Zr(C_6H_6)_2$ molecule, we can compare our computed geometry with previous theoretical results. There is very good agreement between our optimized geometry and those previously reported,[21−25] with a few exceptions which we now note. (1) A B3LYP calculation[24] predicted a considerably larger Zr−C distance (2.56 Å) than our results. This method also predicted a larger Ta−C distance than other theories.[18] Since this functional is also one that we used, the variation is probably due to the difference in basis functions. (2) An MP2 computation[25] predicted a considerably shorter Zr−Bz distance (1.894 Å), and (3) a CCSD(T) calculation[22] predicted longer C−C distances (1.452 Å). Despite these few instances, very good agreement is seen between our theoretically optimized geometry and those previously reported.

The $Hf(C_6H_6)_2$ complex has been previously studied theoretically,[21−23,25] but D_{6d} symmetry was not considered. Our calculations predicted a D_{6h} symmetry with a $^1A_{1g}$ ground electronic state to be the correct geometry, lying slightly less than 1 kcal/mol lower in energy than the D_{6d} isomer by both theoretical methods. The singlet state has also been previously predicted as the ground state for this molecule.[21,23,25] Our calculations predicted a ΔE_{rxn} of 110 and 83 kcal/mol by the BPW91 and B3LYP methods, respectively. Note that both methods predicted the $Zr(C_6H_6)_2$ molecule to be the most stabilized during formation, followed by the hafnium and titanium bisbenzene molecules. Experimentally, the $Hf(C_6H_6)_2$ compound is known to have the largest (67 kcal/mol) binding energy of the Group 4 $M(C_6H_6)_2$ compounds.[22]

Our theoretical methods predicted Hf−C bond lengths of 2.410 and 2.423 Å, Hf−Bz distances of 1.935 and 1.956 Å, and C−C bond distances of 1.437 and 1.429 Å by the BPW91 and B3LYP methods, respectively. These values are all in good agreement with previous predictions.[21−23,25] Zirconium and hafnium M−C and M−Bz distances are predicted to be larger than those for titanium by both methods, attributed to the increase in atomic size of the metal atom. Atomic zirconium and hafnium have almost identical sizes; however, hafnium is predicted to be closer to the benzene ring than zirconium. This indicates that hafnium binds more strongly to benzene, and accordingly the C−C bond distance is predicted to increase in the order $Ti(C_6H_6)_2 < Zr(C_6H_6)_2 < Hf(C_6H_6)_2$, indicating a weakening of the aromatic carbon skeleton.

Our $Zr_2(C_6H_6)_3$ computation confined to a D_{6h} structure converged in a $^1A_{1g}$ ground electronic state. However, our theoretical methods proved to be too demanding to compute vibrational frequencies. Therefore, the structure was reoptimized using the same functionals, but with a smaller 6-31G(d) basis[58] on the carbon and hydrogen atoms, and frequencies were then computed at this level. At this lower level of theory our BPW91 calculations predicted Zr−C bond lengths of 2.491 and 2.405 Å, C−C lengths of 1.463 and 1.442 Å, and C−H lengths of 1.089 and 1.092 Å, where the first number of each set corresponds to values for the center benzene ring. Our B3LYP results were similar predicting Zr−C lengths of 2.502 and 2.410 Å, C−C lengths of 1.454 and 1.434 Å, and C−H bond lengths of 1.082 and 1.085 Å. We should note for comparison that the optimized structure computed with the larger 6-311++G(d,p) basis set for carbon and hydrogen atoms produced shorter lengths for all these reported distance. The ΔE_{rxn} computed with the smaller basis sets were 232 and 179 kcal/mol with the BPW91 and B3LYP methods, respectively.

Relatively little is known about the monobenzene $M(C_6H_6)$ complexes. We begin by discussing the $Zr(C_6H_6)$ complex. Both of our density functionals predicted the $^3A_2$ state with C_{2v} symmetry to be the ground electronic state. One previous theoretical study predicted the $^3E_2$ state (confined to C_{6v} symmetry) to be the ground electronic state of this complex.[25] The quintet state was predicted to be 5 and 3 kcal/mol higher in energy, and the singlet state to be 1 and 13 kcal/mol higher in energy by the BPW91 and B3LYP methods, respectively. The singlet and quintet states optimized to a near C_{6v} symmetry when confined to C_{2v} symmetry, whereas the triplet state showed a larger geometrical deviation in the carbon skeleton. Since the quintet state was predicted to be relatively close in energy to the triplet state by both methods, it is possible that either the triplet or quintet states could be the ground electronic state of the $Zr(C_6H_6)$ complex. As mentioned previously, the observed isotopic splittings of the ν_{i-p}(CH) and ν(CC) mode indicates that this complex does not have C_{6v} symmetry. In addition, the quintet state overestimated the observed vibrational frequencies of this complex, predicting the ν_s(CC) mode at 945.1 and 964.1 cm^{-1}, the ν_{i-p}(CH) vibration at 981.5 and 1005.4 cm^{-1}, and the ν(CC) mode at 1414.7 and 1461.3 cm^{-1} using the BPW91 and B3LYP methods, respectively. As shown in Table 2, the triplet state did a considerably better job predicting these vibrational frequencies. The isotopic shifts of these modes were predicted to be similar in all three electronic states. Despite this, the electronic and vibrational differences between the calculated triplet and quintet states lead us to believe that the $^3A_2$ state is the ground electronic state of the $Zr(C_6H_6)$ complex.

The ΔE_{rxn} for the $Zr(C_6H_6)$ complex was predicted to be 37 and 47 kcal/mol calculated at the BPW91 and B3LYP levels, respectively. In C_{2v} symmetry, our optimized structure had Zr−C lengths of 2.378(4) and 2.276(2) Å calculated with the BPW91 functional and 2.396(4) and 2.294(2) Å at the B3LYP level of theory, where the number in parentheses indicates the number of bonds in the complex corresponding to that length. The C−C bond lengths were computed to be 1.463(4) and 1.416(2) Å with the BPW91 method while lengths of 1.455(4) and 1.406(2) Å were computed with the B3LYP functional. Notice that the average C−C bond lengths (1.447 Å with the BPW91 method and 1.439 Å at the B3LYP level of theory) are larger than the C−C bond lengths in the bisbenzene $Zr(C_6H_6)_2$ compound.

The $Hf(C_6H_6)$ complex was also predicted by both methods to have a $^3A_2$ electronic ground state with C_{2v} symmetry. The quintet state was found to be 8 and 9 kcal/mol higher in energy and the singlet state was predicted to be 15 and 18 kcal/mol higher in energy than the triplet state at the BPW91 and B3LYP levels of theory, respectively. Again the singlet and quintet states showed only minor geometrical deviations when confined in C_{2v} symmetry. A previous theoretical study predicted the $^1A_1$ state to be the ground electronic state of this complex.[25] From this zero-point energy analysis, it is evident that the singlet state is probably not the correct ground electronic state and that the triplet state is more likely to be it. However, at this time we will still consider the quintet state as a possible ground state. In looking at the ν_s(CC) stretching vibrational mode, the quintet state predicted a larger frequency (939.9 cm^{-1} with the BPW91 method and 957.7 cm^{-1} with the B3LYP functional) than the observed vibration at 910.2 cm^{-1}. In addition, the quintet state predicted a larger H/D ratio (1.048 by both methods) than the observed shift (1.040). However, we see in Table 3 that the triplet state did a better job predicting this vibration and isotopic shifts. The only other observed vibrational mode of the $Hf(C_6H_6)$ complex is the ν_{i-p}(CH) mode at 930.2 cm^{-1}. The quintet state predicted this absorption at 974.6 and 996.0 cm^{-1} with H/D isotopic ratios of 1.258 and 1.253 (BPW91 and B3LYP respectively), again overestimating the vibrational frequency and H/D ratio. Also, two absorption peaks were observed for the ν(CC) mode when deuterated benzene was used in experiments, indicating that the carbon ring is nonplanar. The only computation we did that predicted a noteworthy deformation was when the $Hf(C_6H_6)$ complex was in the triplet electronic state. Hence, we do believe the $^3A_2$ state is the correct ground electronic state of the $Hf(C_6H_6)$ complex.

Our calculation predicted a ΔE_{rxn} of 43 and 24 kcal/mol at the BPW91 and B3LYP levels of theory, respectively. Notice that the BPW91 method predicted that $Hf(C_6H_6)$ is more stabilized and B3LYP predicted that it is less stabilized than $Zr(C_6H_6)$ during complexation. Theoretically optimized geometries gave Hf−C lengths of 2.426(4) and 2.294(2) Å and C−C bond lengths of 1.457(4) and 1.406(2) Å using the BPW91 method. B3LYP calculations gave Hf−C lengths of 2.440(4) and 2.305(2) Å and C−C bond lengths of 1.451(4) and 1.397(2) Å.

Although no vibrational modes corresponding to the $Ti(C_6H_6)$ complex were observed in our spectra, theoretical calculations were still performed and they merit comment. Our BPW91 calculations predicted the triplet state to be the ground electronic state with the quintet state lying 4 kcal/mol higher in energy and the singlet state lying 11 kcal/mol higher in energy. Our B3LYP results predicted the quintet state to be the ground electronic state with the triplet state lying less than 1 kcal/mol higher in energy and the singlet state lying 15 kcal/mol higher in energy. Previously, both the triplet[25,38] and the quintet states[27,32,39−41] have been theoretically predicted as the ground state, but experimental evidence indicates that the triplet state may be lower in energy.[40] In our previous study of the reaction products formed between Group 5 transition metals and benzene, we predicted the ground electronic state by comparing our observed spectra and isotopic shifts with those computed. We found that the BPW91 method predicted the correct ground electronic state for all three $M(C_6H_6)$ complexes, whereas the B3LYP method correctly calculated the ground state for only the $Nb(C_6H_6)$ complex.[18] This leads us to believe that the $^3A_2$ state might be the ground electronic state of the $Ti(C_6H_6)$ complex. Since this $^3A_2$ state is the ground state of the $Zr(C_6H_6)$ and $Hf(C_6H_6)$ complexes, it seems probable that the $Ti(C_6H_6)$ complex should also be in this state. However, experimental evidence also indicates that the $Ti(C_6H_6)$ complex has near C_{6v}

symmetry.[40] As the triplet state showed a geometrical deformation in C_{2v} symmetry, this indicates that the quintet state may be the ground state of this complex. The dipole of the $Ti(C_6H_6)$ molecule was found to be 2.4 ± 0.3 D.[40,42] Our theoretical methods overestimated this observation, predicting dipoles of 2.79 and 3.55 D for the triplet state calculated with the BPW91 and B3LYP methods, respectively, and of 2.96 D calculated for the quintet state by both theoretical methods. As we can provide no experimental data of the $Ti(C_6H_6)$ complex, we are unable to comment further on the correct ground state at this time.

Assuming the $^3A_2$ state (C_{2v} symmetry) is the ground electronic state of the $Ti(C_6H_6)$ complex, calculations predicted the ΔE_{rxn} to be 44 kcal/mol by the BPW91 method and 18 kcal/mol by the B3LYP method. Note that the BPW91 method predicted this $Ti(C_6H_6)$ complex to be the most stabilized followed by the $Hf(C_6H_6)$ and $Zr(C_6H_6)$ complexes. B3LYP calculations predicted the binding energy in the opposite order. It is plausible that since the $Ti(C_6H_6)$ complex was not observed in our experiments, and as the $Ti(C_6H_6)_2$ molecule was predicted to be the least stabilized of the Group 4 $M(C_6H_6)_2$ compounds, that $Ti(C_6H_6)$ has the smallest binding energy of the three $M(C_6H_6)$ complexes. Our BPW91 calculations predicted Ti−C bond lengths of 2.236(4) and 2.127(2) Å and C−C bond lengths of 1.461(4) and 1.410(2) Å. B3LYP computations gave slightly different results, predicting Ti−C lengths of 2.269(4) and 2.148(2) Å and C−C lengths of 1.456(4) and 1.396(2) Å. Notice that the C−C bond lengths are predicted to increase in the order Hf < Ti < Zr for the $M(C_6H_6)$ complexes. This trend is different than the trend observed for the $M(C_6H_6)_2$ complexes and is not what we expected. For Group 5 $M(C_6H_6)$ and $M(C_6H_6)_2$ complexes, the C−C bond lengths increase going down the group.[18] Looking at the ν_s(CC) stretching vibrations, we observed these absorptions at 947.0, 933.7, and 928.8 cm^{-1} for the Ti, Zr, and Hf $M(C_6H_6)_2$ complexes, respectively. This indicates a decrease in the C−C bond strength moving down the Group 4 transition series as the optimized geometries predicted. For the $M(C_6H_6)$ complexes, we observe the ν_s(CC) modes at 918.3 and 910.2 cm^{-1} for the zirconium and hafnium complexes, respectively. This shows that even though theoretical predictions indicate that the C−C bond should be stronger for the $Hf(C_6H_6)$ complex, experimentally it is weaker. Hence, we believe that C−C bonds get weaker and M−C bonds get stronger moving down the Group 4 transition series. These observed ν_s(CC) modes are all at lower frequencies than those observed for the complementary Group 5 $M(C_6H_6)$ and $M(C_6H_6)_2$ complexes,[18] indicating that Group 4 transition metals bind more strongly to benzene weakening the aromatic C−C bonds.

Conclusions

Reaction products formed between Group 4 transition metals and benzene have been isolated in an argon matrix and studied by infrared spectroscopy and DFT calculations. The primary reaction products are the $M(C_6H_6)$ and $M(C_6H_6)_2$ complexes. Isotopic substitution of the benzene precursor confirms our molecular and vibrational mode assignments. Based on the observed and calculated isotopic shifts, we believe the sandwich $M(C_6H_6)_2$ compounds have a $^1A_{1g}$ ground electronic state. The $Zr(C_6H_6)$ and $Hf(C_6H_6)$ complexes are computed to have a $^3A_2$ ground state and a non-C_{6v} symmetry. The observed splitting of formerly doubly degenerate modes in the benzene precursor provides the first experimental evidence for a deformation of the carbon skeleton upon early transition metal atom complexation.

Acknowledgment. We gratefully acknowledge the National Science Foundation (NSF) for support of this research under Grant CHE 03-52487 and fellowship support under NSF IGERT Grant 99-72797 for J.T.L.

References and Notes

(1) Nakajima, A.; Kaya, K. *J. Phys. Chem. A* **2000**, *104*, 176.
(2) Andrews, M. P.; Mattar, S. M.; Ozin, G. A. *J. Phys. Chem.* **1986**, *90*, 744.
(3) Andrews, M. P.; Huber, H. X.; Mattar, S. M.; McIntosh, D. F.; Ozin, G. A. *J. Am. Chem. Soc.* **1983**, *105*, 6170.
(4) Mattar, S. M.; Sammynaiken, R. *J. Chem. Phys.* **1997**, *106*, 1080.
(5) Cirelli, G.; Russu, A.; Wolf, R.; Rudin, M.; Schweiger, A.; Gunthard, Hs. H. *Chem. Phys. Lett.* **1982**, *92*, 223.
(6) Andrews, M. P.; Ozin, G. A. *J. Phys. Chem.* **1986**, *90*, 1245.
(7) McCamley, A.; Perutz, R. N. *J. Phys. Chem.* **1991**, *95*, 2738.
(8) Boyd, J. W.; Lavoie, J. M.; Gruen, D. M. *J. Chem. Phys.* **1974**, *60*, 4088.
(9) Efner, H. F.; Tevault, D. E.; Fox, W. B.; Smardzewski, R. R. *J. Organomet. Chem.* **1978**, *146*, 45.
(10) Shobert, A. L.; Hisatsune, I. C.; Skell, P. S. *Spectrochim. Acta* **1984**, *40A*, 609.
(11) Ball, D. W.; Kafafi, A. H.; Hauge, R. H.; Maargrave, J. L. *J. Am. Chem. Soc.* **1986**, *108*, 6621.
(12) Cloke, F. G. N.; Green, M. L. H. *J. Chem. Soc., Dalton Trans.* **1981**, 1938.
(13) Kim, H. S.; Kim, K. *Chem. Phys. Lett.* **1996**, *250*, 192.
(14) Judai, K.; Sera, K.; Amatsutsumi, S.; Yagi, K.; Yasuike, T.; Yabushita, S.; Nakajima, A.; Kaya, K. *Chem. Phys. Lett.* **2001**, *334*, 277.
(15) Benfield, F. W. S.; Green, M. L. H.; Ogden, J. S.; Young, D. *J. Chem. Soc., Chem. Commun.* **1973**, 866.
(16) Anthony, M. T.; Green, M. L. H.; Young, D. *J. Chem. Soc., Dalton Trans.* **1975**, 1419.
(17) Manceron, L.; Andrews, L. *J. Am. Chem. Soc.* **1988**, *110*, 3840.
(18) Lyon, J. T.; Andrews, L. *J. Phys. Chem. A* **2005**, *109*, 431.
(19) (a) Kandalam, A. K.; Rao, B. K.; Jena, P.; Pandey, R. *J. Chem. Phys.* **2004**, *120*, 10414. (b) Sohnlein, B. R.; Li, S.; Yang, D.-S. *J. Chem. Phys.* **2005**, *123*, 214306.
(20) Kambalapalli, S.; Ortiz, J. V. *J. Phys. Chem. A* **2004**, *108*, 2988.
(21) King, W. A.; Di Bella, S.; Lanza, G.; Khan, K.; Duncalf, D. J.; Cloke, F. G. N.; Fragala, I. L.; Marks, T. J. *J. Am. Chem. Soc.* **1996**, *118*, 627.
(22) Hong, G.; Dolg, M.; Li, L. *Int. J. Quantum Chem.* **2000**, *80*, 201.
(23) Dolg, M. *J. Chem. Inf. Comput. Sci.* **2001**, *41*, 18.
(24) Rayane, D.; Allouche, A.-R.; Antoine, R.; Broyer, M.; Compagnon, I.; Dugourd, P. *Chem Phys. Lett.* **2003**, *375*, 506.
(25) Hong, G.; Schautz, F.; Dolg, M. *J. Am. Chem. Soc.* **1999**, *121*, 1502.
(26) Li, J.; Bursten, B. E. *J. Am. Chem. Soc.* **1999**, *121*, 10243.
(27) (a) Pandey, R.; Rao, B. K.; Jena, P.; Blanco, M. A. *J. Am. Chem. Soc.* **2001**, *123*, 3799. (b) Pandey, R.; Rao, B. K.; Jena, P.; Blanco, M. A. *J. Am. Chem. Soc.* **2001**, *123*, 7744.
(28) Yasuike, T.; Yabushita, S. *J. Phys. Chem. A* **1999**, *103*, 4533.
(29) Yasuike, T.; Nakajima, A.; Yabushita, S.; Kaya, K. *J. Phys. Chem. A* **1997**, *101*, 5360.
(30) Clack, D. W.; Warren, K. D. *Inorg. Chim. Acta* **1978**, *30*, 251.
(31) Salomon, O.; Reiher, M.; Hess, B. A. *J. Chem. Phys.* **2002**, *117*, 4729.
(32) Kurikawa, T.; Takeda, H.; Hirano, M.; Judai, K.; Arita, T.; Nagao, S.; Nakajima, A.; Kaya, K. *Organometallics* **1999**, *18*, 1430.
(33) Kurikawa, T.; Takeda, H.; Nakajima, A.; Kaya, K. *Z. Phys. D: At., Mol. Clusters* **1997**, *40*, 65.
(34) Cloke, F. G. N.; Dix, A. N.; Green, J. C.; Perutz, R. N.; Seddon, E. A. *Organometallics* **1983**, *2*, 1150.
(35) Bönnemann, H.; Korall, B. *Angew. Chem., Int. Ed. Engl.* **1992**, *31*, 1490.
(36) Tairova, G. G.; Kvashina, E. F.; Krasochka, O. N.; Kichigina, G. A.; Shvetsov, Yu. A.; Lisetskii, E. M.; Atovmyan, L. O.; Borod'ko, Yu. G. *Nouv. J. Chim.* **1981**, *5*, 603.
(37) Krasochka, O. N.; Shestakov, A. F.; Tairova, G. G.; Shvetsov, Yu. A.; Kvashina, E. F.; Ponomarev, V. I.; Atovmyan, L. O.; Borod'ko, Yu. G. *Khim. Fiz.* **1983**, 1459.
(38) Ouhlal, A.; Selmani, A.; Yelon, A. *Chem. Phys. Lett.* **1995**, *243*, 269.
(39) Chaquin, P.; Costa, D.; Lepetit, C.; Che, M. *J. Phys. Chem. A* **2001**, *105*, 4541.
(40) Imura, K.; Ohoyama, H.; Kasai, T. *Chem. Phys. Lett.* **2003**, *369*, 55.
(41) Pandey, R.; Rao, B. K.; Jena, P.; Newsam, J. M. *Chem. Phys. Lett.* **2000**, *321*, 142.
(42) Imura, K.; Ohoyama, H.; Kasai, T. *Chem. Phys.* **2004**, *301*, 183.

(43) (a) Jaeger, T. D.; van Heijnsbergen, D.; Kippenstein, S. J.; von Helden, G.; Meijer, G.; Duncan, M. A. *J. Am. Chem. Soc.* **2004**, *126*, 10981. (b) Jaeger, T. D.; Duncan, M. A. *J. Phys. Chem. A* **2005**, *109*, 3311.

(44) Andrews, L. *Chem. Soc. Rev.* **2004**, *33*, 123.

(45) Frisch, M. J.; Trucks, G. W.; Schlegel, H. B.; Scuseria, G. E.; Robb, M. A.; Cheeseman, J. R.; Zakrzewski, V. G.; Montgomery, J. A., Jr.; Stratmann, R. E.; Burant, J. C.; Dapprich, S.; Millam, J. M.; Daniels, A. D.; Kudin, K. N.; Strain, M. C.; Farkas, O.; Tomasi, J.; Barone, V.; Cossi, M.; Cammi, R.; Mennucci, B.; Pomelli, C.; Adamo, C.; Clifford, S.; Ochterski, J.; Petersson, G. A.; Ayala, P. Y.; Cui, Q.; Morokuma, K.; Malick, D. K.; Rabuck, A. D.; Raghavachari, K.; Foresman, J. B.; Cioslowski, J.; Ortiz, J. V.; Stefanov, B. B.; Liu, G.; Liashenko, A.; Piskorz, P.; Komaromi, I.; Gomperts, R.; Martin, R. L.; Fox, D. J.; Keith, T.; Al-Laham, M. A.; Peng, C. Y.; Nanayakkara, A.; Gonzalez, C.; Challacombe, M.; Gill, P. M. W.; Johnson, B. G.; Chen, W.; Wong, M. W.; Andres, J. L.; Head-Gordon, M.; Replogle, E. S.; Pople, J. A. *Gaussian 98*, revision A.11.4; Gaussian, Inc.: Pittsburgh, PA, 1998.

(46) (a) Becke, A. D. *Phys. Rev. A* **1988**, *38*, 3098. (b) Perdew, J. P.; Wang, Y. *Phys. Rev. B: Condens. Matter Mater. Phys.* **1992**, *45*, 13244.

(47) (a)Becke, A. D. *J. Chem. Phys.* **1993**, *98*, 5648. (b) Lee, C.; Yang, W.; Parr, R. G. *Phys. Rev. B: Condens. Matter Mater. Phys.* **1988**, *37*, 785.

(48) (a) Krishnan, F.; Binkley, J. S.; Seeger, R.; Pople, J. A. *J. Chem. Phys.* **1980**, *72*, 650. (b) Frisch, M. J.; Pople, J. A.; Binkley, J. S. *J. Chem. Phys.* **1984**, *80*, 3265.

(49) Andrae, D.; Haussermann, U.; Dolg, M.; Stoll, H.; Preuss, H. *Theor. Chim. Acta* **1990**, *77*, 123.

(50) Chertihin, G. V.; Andrews, L. *J. Phys. Chem.* **1995**, *99*, 6356.

(51) Chertihin, G. V.; Andrews, L. *J. Phys. Chem.* **1994**, *98*, 5891.

(52) Kushto, G. P.; Souter, P. F.; Chertihin, G. V.; Andrews, L. *J. Chem. Phys.* **1999**, *110*, 9020.

(53) Wilson, E. B., Jr.; Decius, J. C.; Cross, P. C. *Molecular Vibrations;* McGraw-Hill: New York, 1955.

(54) Kurikawa, T.; Hirano, M.; Takeda, H.; Yagi, K.; Hoshino, K.; Nakajima, A.; Kaya, K. *J. Phys. Chem.* **1995**, *99*, 16248.

(55) Hoshino, K.; Kurikawa, T.; Takeda, T.; Nakajima, A.; Kaya, K. *J. Phys. Chem.* **1995**, *99*, 3053.

(56) Hirano, M.; Judai, K.; Nakajima, A.; Kaya, K. *J. Phys. Chem. A* **1997**, *101*, 4893.

(57) Weis, P.; Kemper, P. R.; Bowers, M. T. *J. Phys. Chem. A* **1997**, *101*, 8207.

(58) (a) Petersson, G. A.; Bennett, A.; Tensfeldt, T. G.; Al-Laham, M. A.; Shirley, W. A.; Mantzaris, J. *J. Chem. Phys.* **1988**, *89*, 2193. (b) Petersson, G. A.; Al-Laham, M. A. *J. Chem. Phys.* **1991**, *94*, 6081.